Supporting Information

Interfacial electron modulation of RuO_2@NiO enables efficient hydrazine-assisted hydrogen production in alkaline seawater

Boxue Wang,[a] Huachuan Sun,*[a] Mingpeng Chen,[a] Tong Zhou,[a] Hongshun Zheng,[a] Minghui Shi,[a] Dequan Li,[a] Yuewen Wu,[a] Yumin Zhang,[a] Jin Zhang,[a] Hao Cui,[b] Qingju Liu*[a]

[a]National Center for International Joint Research of Photoelectric Energy Materials and Application, Yunnan Key Laboratory for Micro/Nano Materials & Technology, School of Materials and Energy, Yunnan University, Kunming 650091, China.

[b]Yunnan Precious Metals Laboratory Co., Ltd., Kunming, 650106, P. R. China.

† Footnotes relating to the title and/or authors should appear here.

* Corresponding author.

1. Experimental section

1.1. Chemicals

The nickel(II) nitrate hexahydrate ($Ni(NO_3)_2·6H_2O$, analytical reagent (AR), ≥ 98%), hexamethylenetetramine ($C_6H_{12}N_4$, HMT), ruthenium(III) chloride hydrate ($RuCl_3·xH_2O$, 35.0–42.0% Ru basis), and potassium hydroxide (KOH, AR, ≥ 85%) were purchased from Aladdin (Shanghai, China). The commercial Pt/C (20 wt%) and nickel foam (NF) were purchased from Suzhou Sinero Technology Co., Ltd. The absolute ethanol and hydrochloric acid (HCl, 36%–38%) were purchased from Chengdu Kelong Chemical Co. Ltd. Nafion solution (5 wt%) was obtained from Sigma-Aldrich. Hydrazine hydrate ($N_2H_4·H_2O$, 80%) was purchased from Chongqing Chuandong Chemical (Group) Co., Ltd. In addition, the natural seawater was collected from the Bohai Sea (latitude 40.6179° N, longitude 120.8107° E) and subjected only to a simple filtration before use. All the chemicals were used directly without any purification. Deionized (DI) water with a resistivity of 18.2 MΩ cm was used during the experiments.

1.2. Pretreatment of NF

Several pieces of NF with a size of 2 × 4 cm^2 were sequentially ultrasonically cleaned in 3 M HCl, deionized (DI) water, and ethanol for 8, 5, and 5 min, respectively, and then naturally dried at room temperature to obtain clean NF.

1.3. Preparation of $Ni(OH)_2$/NF

Self-supported $Ni(OH)_2$/NF precursors were synthesized via a one-step hydrothermal method. Typically, $Ni(NO_3)_2·6H_2O$ (1.6 g) and HMT (1.6 g) were dissolved in DI water (40 mL) and ultrasonicated for 20 min to form a homogeneous solution. The solution was then transferred to a Teflon-lined stainless-steel autoclave, and the pretreated NF was immersed in the solution. The hydrothermal reaction was carried out at 110 ℃ for 12 h. After naturally cooling to room temperature, the obtained sample was taken out, thoroughly rinsed with DI water and ethanol, and dried to yield $Ni(OH)_2$/NF.

1.4. Preparation of NiO/NF

NiO/NF was obtained by annealing the as-prepared $Ni(OH)_2$/NF precursor in air at 300 ℃ for 3 h.

1.5. Preparation of RuO_2@NiO/NF and RuO_2/NF

RuO_2@NiO/NF was prepared via an impregnation-annealing process. Specifically, the $Ni(OH)_2$/NF precursor was immersed in an aqueous $RuCl_3 \cdot xH_2O$ solution (4 mg mL^{-1}) at room temperature for 24 h. After impregnation, the sample was rinsed with DI water and ethanol, dried, and then annealed in air at 300 ℃ for 3 h to obtain RuO_2@NiO/NF-4 (denoted as RuO_2@NiO/NF). The mass loading on the NF was determined to be 1.57 mg cm^{-2} by measuring the weight of the sample before and after preparation. For comparison, the $RuCl_3 \cdot xH_2O$ concentration was adjusted to 2 and 6 mg mL^{-1} under identical conditions, and the resulting samples were denoted as RuO_2@NiO/NF-2 and RuO_2@NiO/NF-6, respectively. To investigate the effect of annealing temperature, the annealing temperature was varied to 200 °C and 400 °C while keeping other conditions unchanged, and the resulting samples were denoted as RuO_2@NiO/NF-T200 and RuO_2@NiO/NF-T400, respectively. For reference, RuO_2/NF was fabricated following the same impregnation-annealing procedure as RuO_2@NiO/NF, except that the $Ni(OH)_2$/NF precursor was directly replaced with pristine NF.

1.6. Preparation of Pt/C

Typically, 5 mg commercial Pt/C (20 wt%) was dispersed in a mixture solution of 400 μL DI water, 560 μL absolute ethanol, and 40 μL Nafion solution, and then ultrasonicated to form a homogeneous ink. Pt/C electrodes were obtained by uniformly dropping 200 μL of ink onto the treated NF (1 × 1 cm^2) and then drying overnight at room temperature.

2. Material characterizations

X-ray diffraction (XRD) patterns were collected on a Rigaku TTRIII-18 kW diffractometer using Cu Kα radiation (λ = 1.5406 Å) with a scan rate of 5° min^{-1} over 20–80°. Raman spectra were recorded on a confocal Raman spectrometer (HORIBA XploRA PLUS) with a laser excitation at λ = 532 nm over the range of 200–1400 cm^{-1}.

X-ray photoelectron spectroscopy (XPS) was performed on a Thermo Scientific K-Alpha+ spectrometer equipped with a monochromatic Al Kα source (hν = 1486.6 eV). All spectra were acquired under identical conditions and calibrated to the C 1s peak at 284.8 eV. The morphology and microstructure were characterized by field-emission scanning electron microscopy (FEI Nova NanoSEM 450) and transmission electron microscopy (TEM/HRTEM, JEOL JEM-F200); elemental mappings were obtained by STEM-EDS. Inductively coupled plasma optical emission spectrometry (ICP-OES, Agilent 5110) and ion chromatography (IC, Thermo Scientific ICS-1100) were employed for elemental and chloride quantification, respectively.

3. Electrochemical measurements

The electrochemical performance of the prepared samples was measured in a typical three-electrode system using CHI 1140C and CHI 760E electrochemical workstations. Specifically, the reference electrode, counter electrode, and working electrode were Hg/HgO, carbon rod, and the synthesized samples (1 × 1 cm^2), respectively. All electrochemical tests were conducted in an alkaline seawater (1M KOH +seawater) or alkaline seawater containing hydrazine (1.0 M KOH + 0.5 M N_2H_4) at a sweep rate of 5 mV s^{-1}. After KOH addition, the Cl^- concentrations in the alkaline seawater electrolytes (with/without 0.5 M N_2H_4) were determined by IC to be 0.486 and 0.494 mol L^{-1}, respectively. All potentials were normalized to the reversible hydrogen electrode (RHE). All potentials were converted to the RHE scale at 25 °C using a Hg/HgO (1.0 M KOH) reference electrode according to $E_{RHE} = E^{0}_{Hg/HgO} + 0.0591 \times pH$ (0.098 V vs SHE at 25 °C). Unless otherwise stated, all potentials in this work are reported vs RHE. The ohmic drop was compensated using the built-in *iR* compensation function of the CHI electrochemical workstation (positive feedback mode). The solution resistance R was automatically determined by the instrument (via a small-amplitude perturbation) prior to polarization measurements, and 95% *iR* compensation was applied to avoid potential overcompensation/instability at high current densities. The corrected potential was calculated as $E_{corrected} = E_{measured} - 0.95iR$. The double-layer

capacitance (C_{dl}) was calculated by measuring cyclic voltammetry (CV) at different sweep rates (100, 120, 140, 160, and 180 mV s^{-1}) during the non-Faradaic region. The charge transfer resistance (Rct) was obtained by measuring electrochemical impedance spectroscopy (EIS) in the frequency range from 10000 to 0.01 Hz.

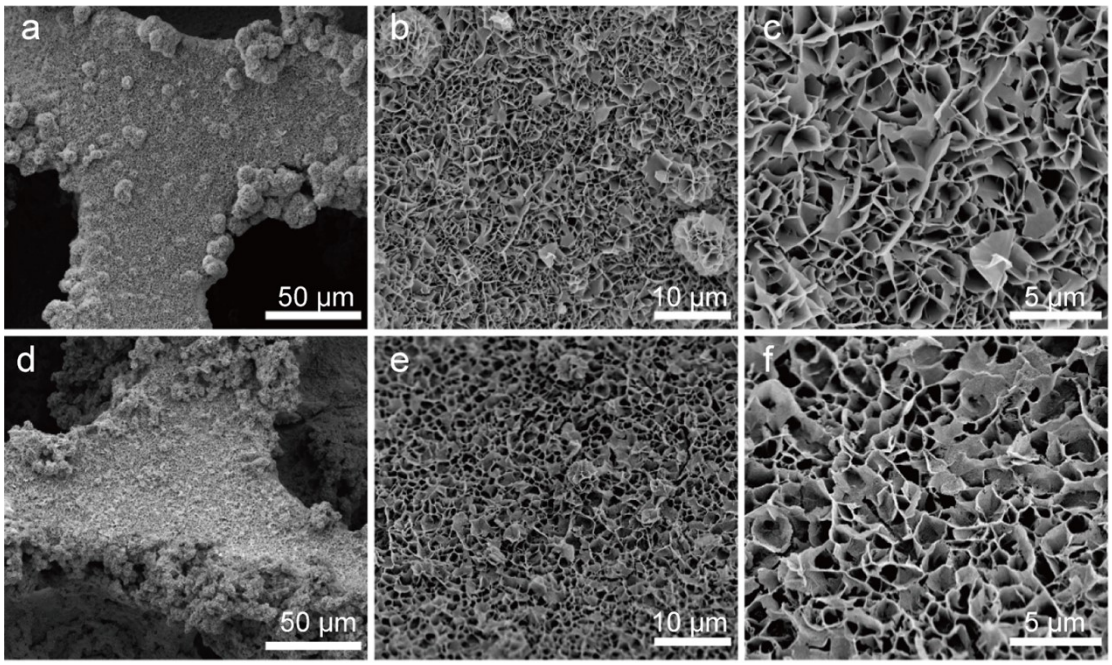

Fig. S1 SEM images of (a–c) NiO/NF and (d–f) RuO_2@NiO/NF at different magnifications.

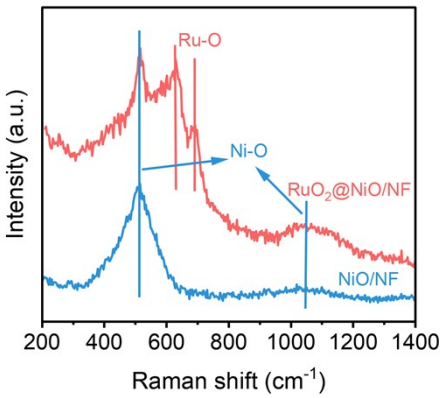

Fig. S2 Raman spectra of NiO/NF and RuO_2@NiO/NF.

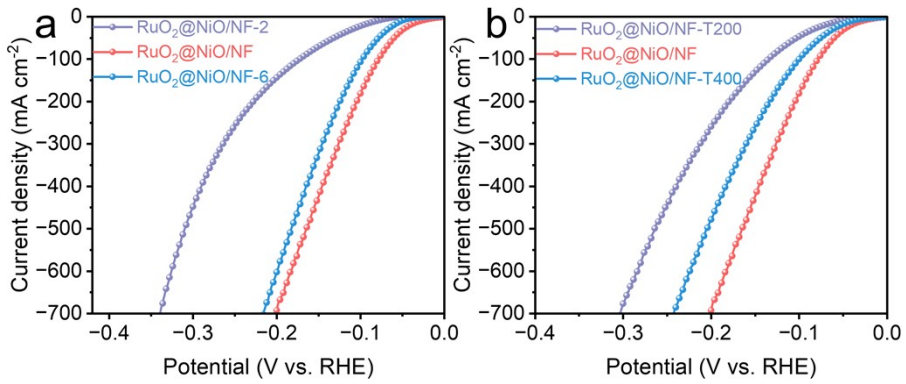

Fig. S3 LSV curves of (a) RuO_2@NiO/NF-2, RuO_2@NiO/NF, and RuO_2@NiO/NF-6 and (b) RuO_2@NiO/NF-T200, RuO_2@NiO/NF, and RuO_2@NiO/NF-T400.

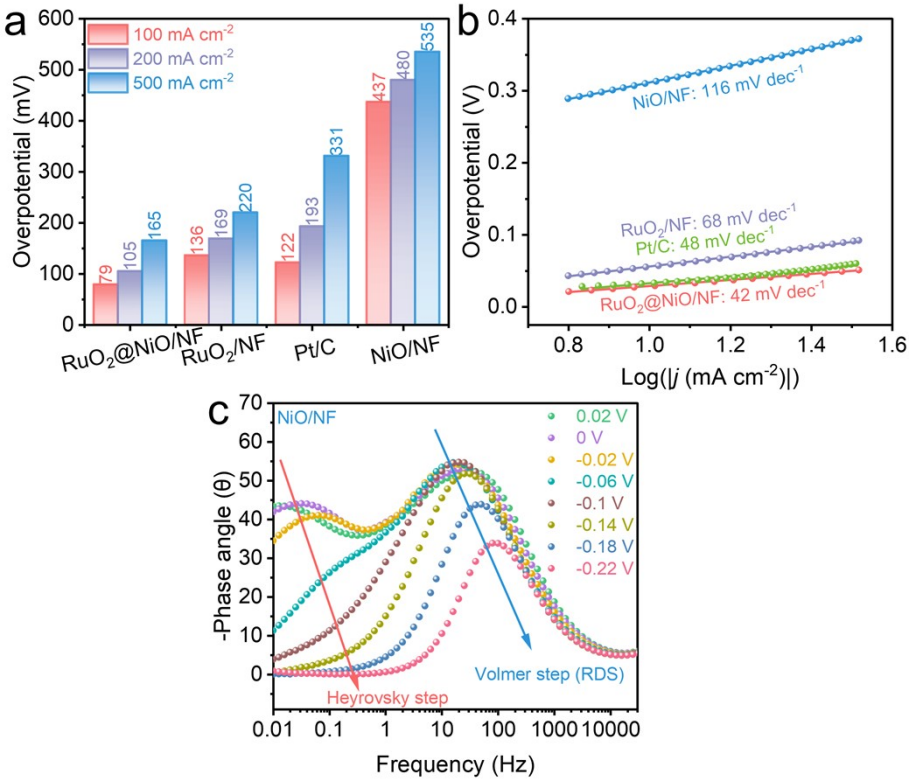

Fig. S4 (a) The overpotentials of RuO_2@NiO/NF, RuO_2/NF, NiO/NF, and Pt/C at different current densities. (b) Tafel slopes of RuO_2@NiO/NF, RuO_2/NF, NiO/NF, and Pt/C. (c) In situ Bode phase plots of NiO/NF.

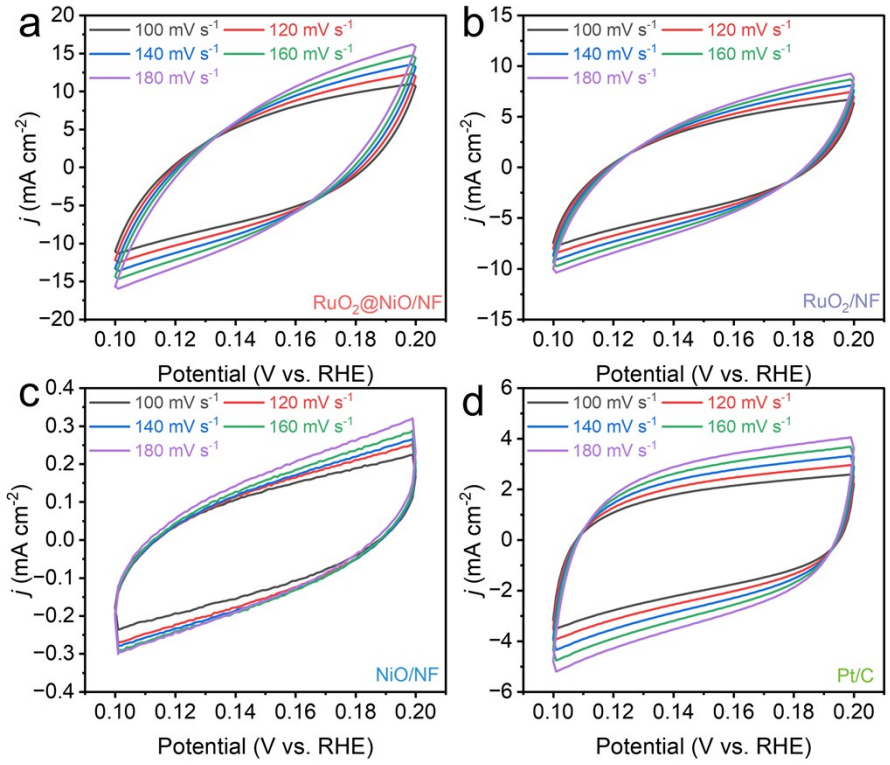

Fig. S5 CV curves of (a) RuO_2@NiO/NF, (b) RuO_2/NF, (c) NiO/NF, and (d) Pt/C.

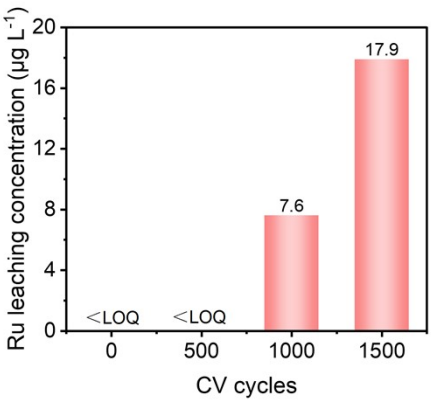

Fig. S6 Ru ion concentration in the electrolyte after different CV cycles during the HER process.

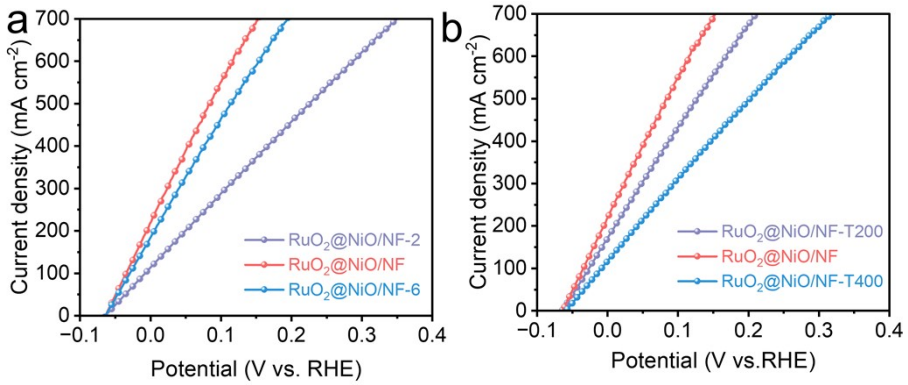

Fig. S7 LSV curves of (a) RuO_2@NiO/NF-2, RuO_2@NiO/NF, and RuO_2@NiO/NF-6 and (b) RuO_2@NiO/NF-T200, RuO_2@NiO/NF, and RuO_2@NiO/NF-T400.

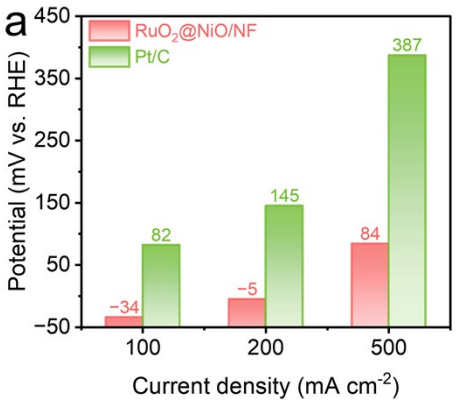

Fig. S8 The potentials of RuO_2@NiO/NF, RuO_2/NF, NiO/NF, and Pt/C at different current densities.

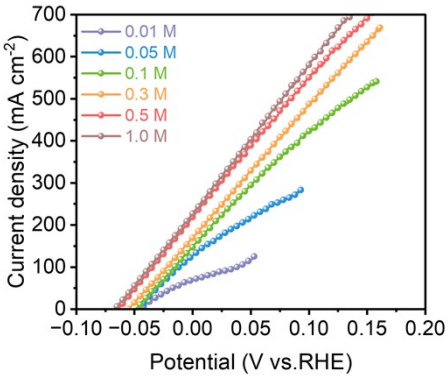

Fig. S9 LSV curves of RuO_2@NiO/NF at different hydrazine concentrations.

Fig. S10 Tafel slopes of RuO_2@NiO/NF, RuO_2/NF, NiO/NF, and Pt/C.

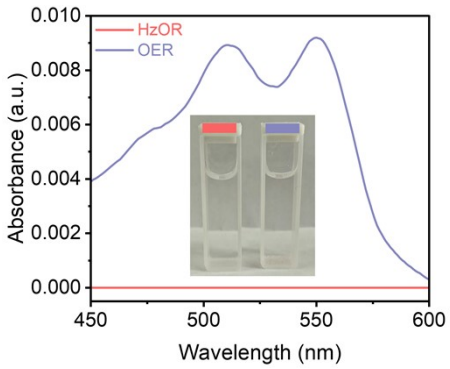

Fig. S11 UV–vis spectra of the electrolyte after 1500 CV cycles under HzOR and OER conditions (DPD method), showing a negligible hypochlorite/free-chlorine signal for HzOR compared with the OER control. Inset: photographs of the corresponding electrolyte solutions.

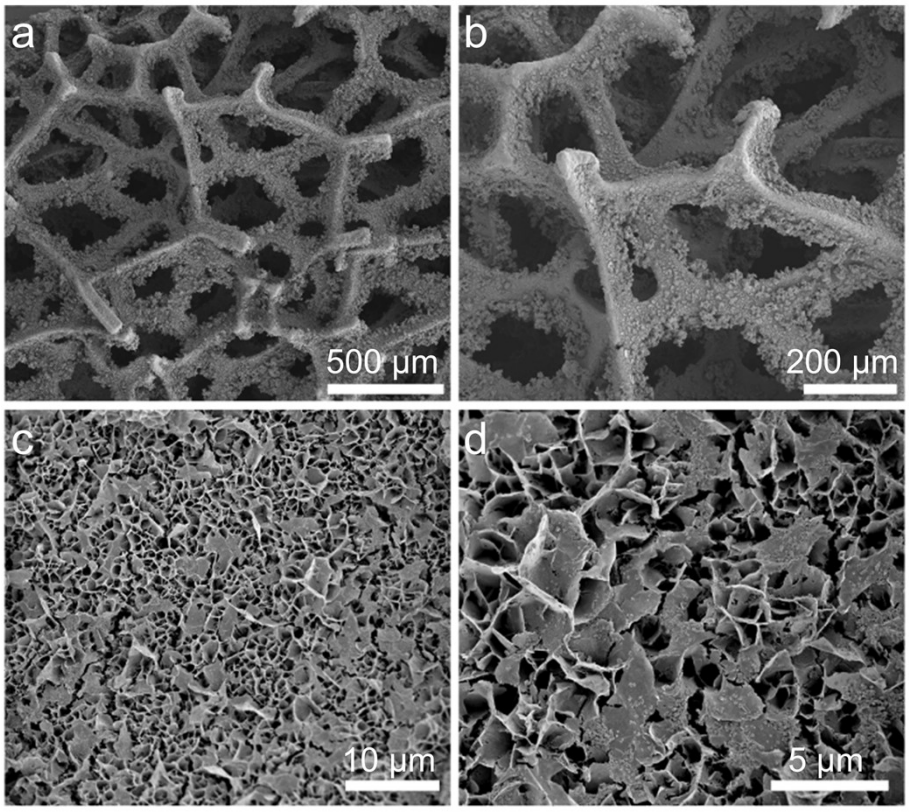

Fig. S12 SEM images of RuO_2@NiO/NF after the stability test.

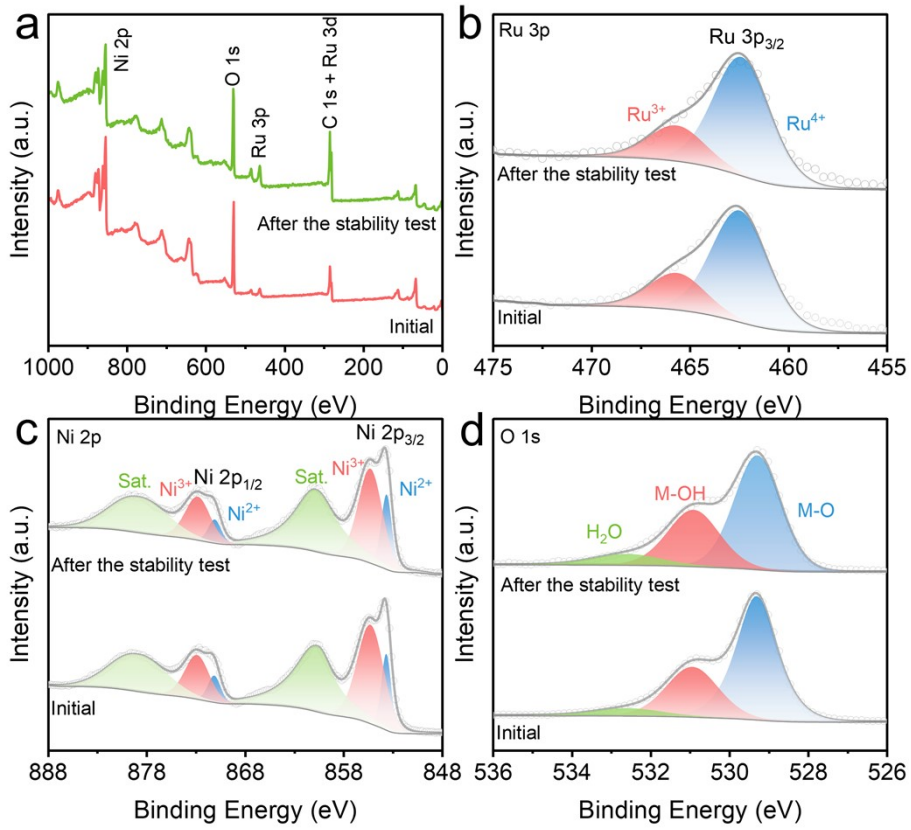

Fig. S13 XPS spectra of RuO_2@NiO/NF before and after the stability test.

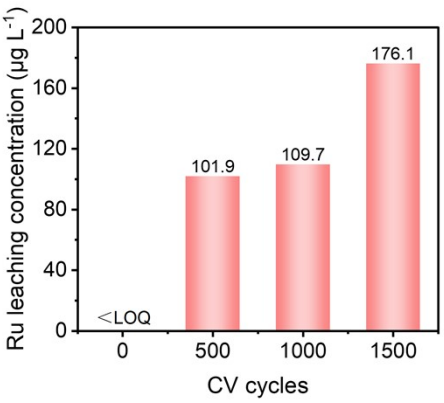

Fig. S14 Ru ion concentration in the electrolyte after different CV cycles during the HzOR process.

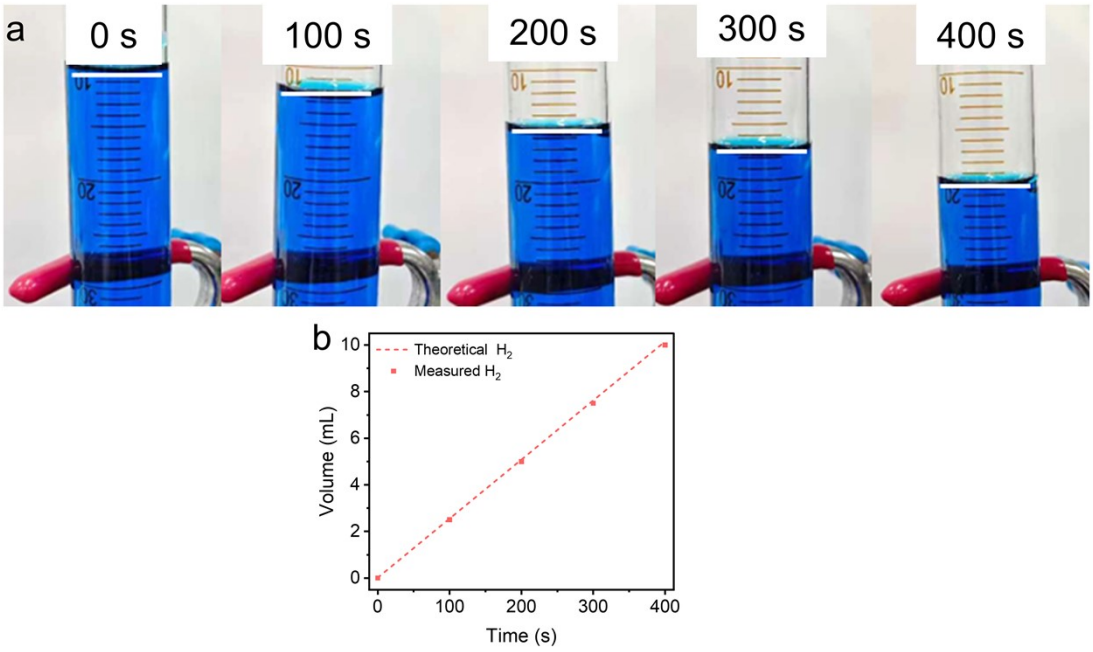

Fig. S15 (a) Experimental device for measuring Faraday efficiency by drainage method. (b) Photographs of gas collection at different times. (c) Theoretical and measured gas production at different times.

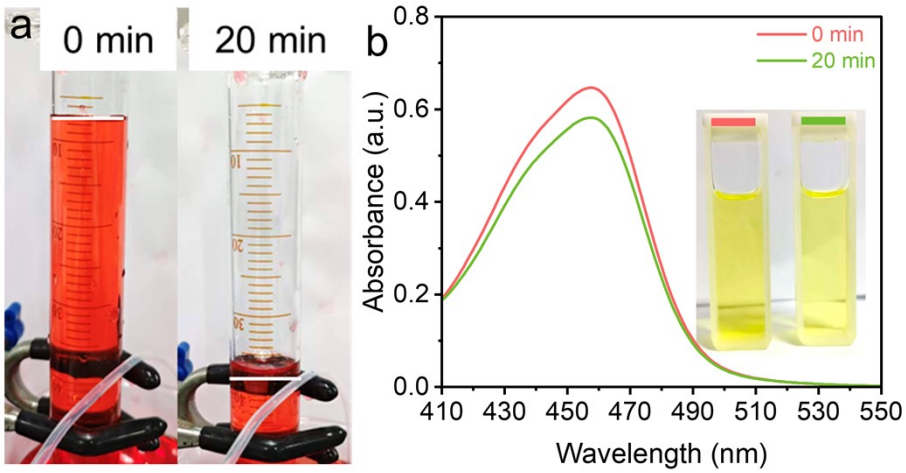

Fig. S16 (a) Photographs of anodic gas collection at 0 and 20 min during HzOR electrolysis. (b) UV–vis spectra (p-DMAB method) of the electrolyte at 0 and 20 min, indicating the decrease in N_2H_4 concentration during operation (inset: photographs of the corresponding solutions).

Table S1. ICP results.

Materials	Ni (wt%)	Ru (wt%)
RuO_2@NiO/NF-2	55.44	9.85
RuO_2@NiO/NF	52.35	11.56
RuO_2@NiO/NF-6	50.29	14.32

Table S2. The mass loading of Ru on RuO_2@NiO/NF.

Materials	Ru loading (mg cm^{-2})
RuO_2@NiO/NF	0.18

Table S3. Comparison of OHzS performance for RuO_2@NiO/NF || RuO_2@NiO/NF with recently reported bifunctional electrocatalysts at 100 mA cm^{-2}.

Catalysts	Cell voltage (mV) @100 mA cm^{-2}	Ref.
RuO_2@NiO/NF	93	This work
CoFeNiCrMnP/NF	94	1
Ru NPs/H-NCMTs	108	2
Ir/PNPC	167	3
Pt/C	206	This work
Ru/NiCo LDH	223	4
NiCoMoS@$Ni(CN)_2$	380	5
ZIF67@CoNiSe-3	450	6
Pt/CoFe/NF	531	7
Mn-Ni_3S_2	634	8

Table S4. IC results of NH_4^+, NO_3^-, and NO_2^- before and after electrolysis.

Ion species	Before electrolysis (mg L^{-1})	After electrolysis (mg L^{-1})	Increase (mmol)
NH_4^+	22.736	25.628	0.003929
NO_3^-	1.203	1.9	0.000281
NO_2^-	0.117	0.441	0.000176

References:

1 K. Li, J. He, X. Guan, Y. Tong, Y. Ye, L. Chen and P. Chen, *Small*, 2023, **19**, 2302130.

2 W. Wang, Q. Qian, Y. Li, Y. Zhu, Y. Feng, M. Cheng, H. Zhang, Y. Zhang and G. Zhang, *ACS Appl. Mater. Interfaces*, 2023, **15**, 26852-26862.

3 L. Wang, Q. Yu, H. Li, S. Zeng, R. Li, Q. Yao, H. Chen, X. Zhang and K. Qu, *Int. J. Hydrogen Energy*, 2024, **90**, 701-709.

4 J. Wei, Y. Song, M. Gan, G. An, Y. Shen, X. Zhao, Y. Zhang, P. Liu, B. Xu and J. Guo, *Sustainable Mater. Technol.*, 2025, **44**, e01413.

5 N. Nwaji, B. Fikadu, M. Osial, Z. M. Goudarzi, S. Asgaran, L. T. Tufa, J. Lee and M. Giersig, *Int. J. Hydrogen Energy*, 2024, **86**, 554-563.

6 W. Liu, T. Shi and Z. Feng, *J. Colloid Interface Sci.*, 2023, **630**, 888-899.

7 T. Yu, G. Liu, T. Nie, Z. Wu, Z. Song, X. Sun and Y.-F. Song, *ACS Catal.*, 2024, **14**, 14937-14946.

8 G. Wang, W. Ren, F. Zhang, K. Ji, J. Wang, J. Yang, X. Li, R. Liu, S. Wang, Y. Ji, Z. Chen, B.-J. Ni, J. Xie, Z. Yang and Y.-M. Yan, *Chem. Eng. J.*, 2025, **523**, 168088.